JOURNAL OF AIRCRAFT
Vol. 33, No. 2, March–April 1996

Dynamic Reattachment on a Downward Pitching Finite Wing

Scott J. Schreck*
U.S. Air Force Office of Scientific Research, Bolling Air Force Base, Washington, DC 20332
William E. Faller†
Johns Hopkins University, Baltimore, Maryland 21218
and
Marvin W. Luttges‡
University of Colorado, Boulder, Colorado 80309

A finite wing was pitched downward at a constant rate from a fully stalled condition to zero angle of attack. Dynamic reattachment on the downward pitching wing was characterized in detail using unsteady surface pressure measurements. Results showed that dynamic reattachment initiation and progression velocity varied in response to alterations in nondimensional pitch rate and span location. In addition, these alterations to reattachment initiation and progression were prominently reflected in normal force data. An empirical model for dynamically separating flowfields was successfully adapted to account for these observed trends. Comparisons between dynamically reattaching and dynamically separating flows were also informative. Characterization and comprehension of three-dimensional dynamic reattachment are crucial prerequisites for control of unsteady separated flowfields generated by rapidly maneuvering aircraft, helicopter rotor blades, and wind energy machines.

Nomenclature

C_n = normal force coefficient
c = wing chord length, cm
c_p = pressure coefficient
$d\alpha/dt$ = pitch rate, rad/s
Re_c = chord Reynolds number
s = wingspan length, cm
t = time, s
t_{nd} = nondimensional time, tU_∞/c
U_∞ = test section velocity, m/s
α = angle of attack, deg
α^+ = nondimensional pitch rate, $c(d\alpha/dt)/U_\infty$

Introduction

THE pervasive occurrence of three-dimensional, unsteady separated flowfields continues to prompt intense study. Rapidly maneuvering aircraft, helicopter rotor blades, and wind energy machines all elicit unsteady separated flowfields. Frequently, unsteady separated flows exercise a pronounced adverse influence upon the effectiveness of these and other systems. If thoroughly understood and properly controlled, three-dimensional unsteady separated flows could be suppressed or even harnessed, thereby dramatically enhancing performance for a broad spectrum of fluid dynamic systems.

Several experiments have examined the three-dimensional, vortex-dominated flowfields generated when wings undergo dynamic separation during pitch up.[1–6] Energetic large-scale vortices are generated and transiently reside on the upper surface of wings dynamically pitched up through the static stall angle of attack. These vortices radically alter the upper surface pressure distributions on a wing and produce greatly amplified aerodynamic forces and moments. Mutual interactions between vortices and accumulations of vorticity deform the vortex, disrupting vortex spanwise uniformity. This yields unsteady surface pressure distributions and spanwise aerodynamic loads that are highly three dimensional.[4,7]

Previous research concerning dynamic separation during wing pitch up has yielded physical comprehension[8] as well as real-time prediction and control[9–11] of three-dimensional, dynamically separated flowfields. However, complete control of systems that mitigate or exploit unsteady aerodynamic effects will also demand understanding of three-dimensional dynamic reattachment. Niven et al.[12] and Niven and Galbraith[13] have examined dynamic reattachment on two-dimensional airfoils pitching down at a constant rate from fully stalled conditions. In these experiments unsteady surface pressure distribution development and aerodynamic force histories varied consistently with changes in dynamic parameters.

In an experiment involving an oscillating airfoil, Ahmed and Chandrasekhara[14] found that dynamic reattachment initiated near the airfoil leading edge, progressed aft over the chord, and completed with the disappearance of a separation bubble. Freymuth[15] has visualized convective removal of a vortex system from the surface of a wing dynamically pitched up and then immediately down. Ericsson[16] has highlighted the importance of understanding unsteady reattachment for controlling rapidly maneuvering aircraft and has analyzed existing experimental results using an empirical model.

To date, dynamic reattachment has not been quantitatively examined for three-dimensional wings. The current investigation employs unsteady surface pressure measurements to quantify unsteady surface pressure distribution and aerodynamic force histories for three-dimensional wings. Data were acquired for seven nondimensional pitch rates at three span locations. This information allowed quantification of three-dimensional dynamic reattachment and enabled the roles of surface pressure gradient and freestream influence to be ascertained.

Experimental Methods

Unsteady surface pressure measurements were performed in the Frank J. Seiler 0.91 × 0.91 m low-speed wind tunnel lo-

Presented as Paper 94-1907 at the AIAA 12th Applied Aerodynamics Conference, Colorado Springs, CO, June 20–23, 1994; received Oct. 24, 1994; revision received Aug. 8, 1995; accepted for publication Sept. 5, 1995.

*Program Manager, 110 Duncan Avenue, Suite B213. Member AIAA.
†Research Faculty, Department of Mechanical Engineering. Member AIAA.
‡Professor, Department of Engineering Sciences. Member AIAA.

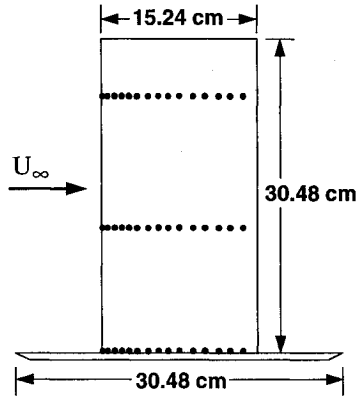

Fig. 1 Schematic of wing-splitter plate configuration showing pressure port locations.

cated at the U.S. Air Force Academy. A rectangular planform wing with 15.24 cm chord length was fabricated from hollow aluminum NACA 0015 airfoil stock. Fifteen miniature pressure transducers were installed inside the hollow wing model. These transducers were close coupled to the wing surface through pressure ports located along the chord line, 3.05 cm inboard of the wing end. Previous tests confirmed the level frequency response to 1 kHz for this installation

Pressure transducer signals were low-pass filtered to prevent aliasing and were amplified by a gain of 1000. These signals were then sampled and digitized with 12-bit resolution by the data acquisition system. The surface pressure measurement system was calibrated before and after acquiring the data presented herein. These calibrations showed that sensitivity drifts did not exceed 0.7% on any of the 15 channels. During data acquisition, zero drifts did not exceed 0.1% of maximum deflection on any channel. Typical drifts in sensitivities and zeroes were substantially less than these maximum values.

A circular aluminum splitter plate, 30.48 cm in diameter and 0.64 cm thick, was machined to a sharp edge around the plate perimeter. The splitter plate had a NACA 0015 cutout centered in it, which allowed it to slide onto the wing and be positioned at arbitrary span locations. To effectively move the pressure ports along the wingspan, the splitter plate was first positioned at the desired distance from the pressure ports. Then, a tip extension of the correct length was added to the wing, bringing the span length to 30.48 cm and maintaining the aspect ratio constant at 2.0. All three tip extensions used in these experiments terminated in a square tip. The chordwise row of pressure ports was successively moved to three span locations, effectively distributing pressure ports over the wing surface as shown in Fig. 1.

Model pitching was driven by a 3.5-hp stepper motor. The wing-splitter plate combination was mounted on a steel shaft 2.86 cm in diameter that was connected to the stepper motor through a gear linkage having a 4:1 reduction ratio. The independent variables explored in the surface pressure experiments included nondimensional pitch rates 0.01, 0.02, 0.05, 0.075, 0.10, 0.15, and 0.20, as well as spanwise pressure port locations 0.0, 0.375, and 0.80 span outboard of the splitter plate. Wing pitch axis was located at 0.25 chord throughout the experiment. For each parameter combination, 20 consecutive wing pitch motions were sampled and ensemble averaged. Test section velocity was held constant at 9.14 m/s, yielding a chord Reynolds number of 6.9×10^4.

Results

Pitching Motions

Angle-of-attack histories for the seven measured nondimensional pitch rates are shown in Fig. 2. All seven histories begin at 60.0 deg and end at 0.0 deg. The beginning of each history coincides with the initiation of surface pressure data acquisition. Thus, the plots in Fig. 2 can be used in conjunction with subsequent plots to determine an instantaneous wing angle of attack. The wing was pitched at a constant rate from 60.0 to 0.0 deg to collect upper surface data and from −60.0 to 0.0 degrees to acquire lower surface data. It should be noted that none of the angle-of-attack histories exhibits prominent nonlinearity or suffers from appreciable acceleration or deceleration transients.

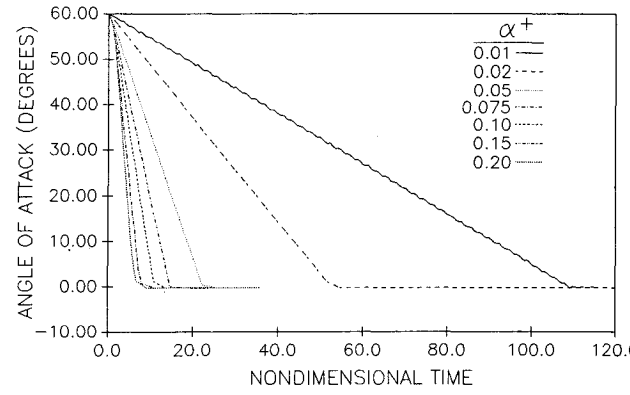

Fig. 2 Angle-of-attack histories for experimental range of nondimensional pitch rate.

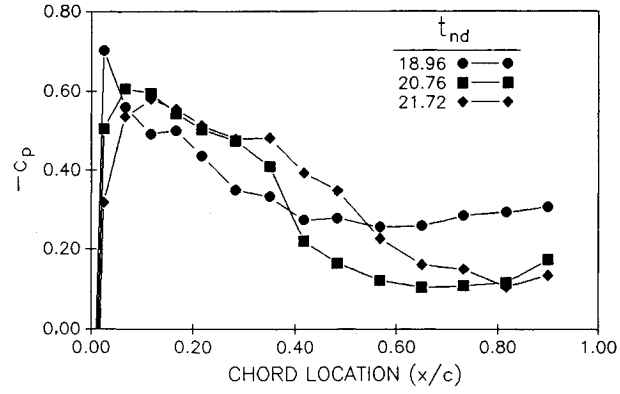

Fig. 3 Representative chordwise surface pressure distributions during reattachment for $\alpha^+ = 0.05$, at 0.00 span.

Surface Pressure Analysis

Figure 3 contains three upper surface chordwise pressure distributions for a nondimensional pitch rate 0.05 at 0.00 span. These plots document instantaneous surface pressure distribution at three nondimensional times during dynamic reattachment. Surface pressures at 0.00 chord have been omitted to obtain improved plot clarity in the chord region of interest. At nondimensional time 18.96, surface pressure gradient was visibly diminished between 0.28–0.90 chord, consistent with flow separation in this chord region. At nondimensional time 20.76, the forward boundary of this separated region had moved downstream as reattachment had progressed aft over the chord. At nondimensional time 21.72, the separated region forward boundary had nearly reached the rearmost pressure port location at 0.90 chord.

Note that the vertical axis is inverted in Fig. 3 and that the peaks in the plots denote pressure minima. As such, pressure gradients between 0.0–0.1 chord are predominantly favorable, while adverse pressure gradients prevail between 0.1–0.6 chord. In contrast to upper surface processes, lower surface chordwise pressure distributions exhibited negligible temporal evolution, and will not be shown graphically herein.

Figure 4 shows upper surface unsteady pressure records for a nondimensional pitch rate 0.05 at 0.00 span. This graph contains 15 surface pressure histories measured at the 15 pressure port locations. Trace 1, at the bottom of the figure, shows

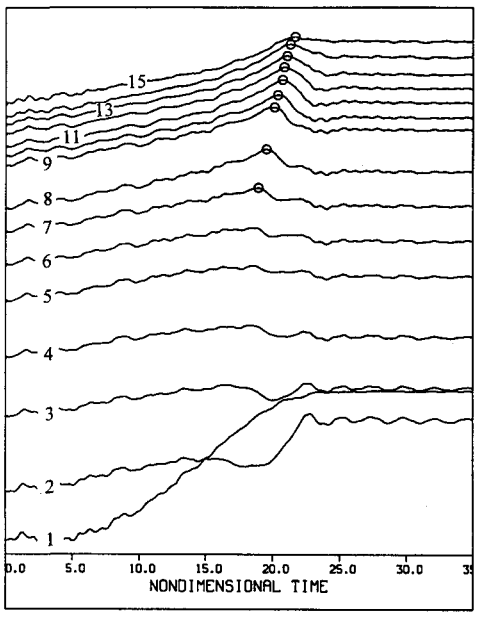

Fig. 4 Representative set of 15 unsteady upper surface pressure histories for $\alpha^+ = 0.05$, at 0.00 span.

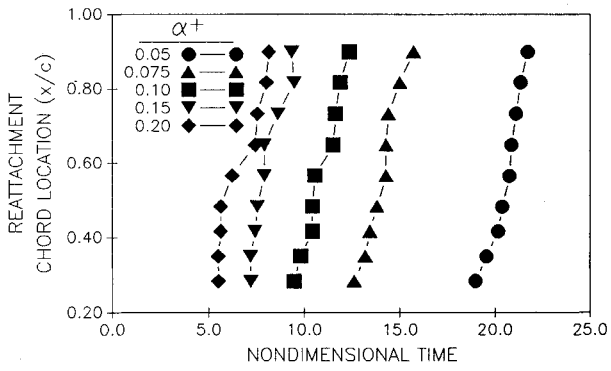

Fig. 5 Representative graph of reattachment chord location vs nondimensional time for $\alpha^+ = 0.05$, at 0.00 span.

surface pressure variation with time at the leading-edge pressure port. Traces 2–15, successively higher on the figure, correspond to pressure port locations progressively farther aft on the wing chord. Nondimensional time 0.0 corresponds to the inception of both wing pitch down and data acquisition. In contrast to Fig. 3, the Fig. 4 vertical axis is not inverted. Thus, the peaks in the Fig. 4 pressure traces correspond to pressure maxima.

Figure 4 shows that surface pressures initially increased at all 15 pressure ports as the wing pitched down. At ports 4–15, the pressure rise rate was uniform and culminated in prominent pressure maxima. At these ports, maximum pressure levels were not exceeded thereafter and can be termed absolute. At ports 4–7, absolute pressure maxima apparently occurred simultaneously, subject to limits imposed by the temporal discretization. Aft of port 7, absolute pressure maxima occurred at later nondimensional times for port locations farther aft on the wing chord, consistent with aftward progressing reattachment. Pressure maxima corresponding to the arrival of reattachment are indicated on traces 7–15 in Fig. 4 by circular symbols. Finally, pressure maxima were followed by falling pressures, with the pressure decrease rate varying substantially over the chord and generally attaining maximum rates near midchord.

Histories documenting the aftward progression of reattachment were extracted from graphs like that shown in Fig. 4. Representative reattachment progression histories are presented in Fig. 5 as plots of reattachment chord location vs nondimensional time, for five nondimensional pitch rates. In accordance with the criteria stated previously, reattachment histories consistently began at 0.28 chord and progressed steadily aftward. Instantaneous aftward progression speed varied with time as evidenced by slope variations in the plots.

Reattachment Initiation

Figure 6 relates angle of attack at which reattachment first occurred on the wing to nondimensional pitch rate for three span locations. At 0.38 and 0.80 span, nondimensional pitch rate 0.10 delayed reattachment to the lowest angles of attack. At these span locations, nondimensional pitch rates both higher and lower than 0.10 yielded reattachment inception at higher angles. A similar trend was seen at the splitter plate, at 0.00 span. Here, nondimensional pitch rate 0.15 delayed reattachment to the lowest angle of attack. Lower as well as higher nondimensional pitch rates again caused reattachment to initiate at higher angles of attack. Across the experimental range of nondimensional pitch rate, reattachment generally was delayed to the lowest angles of attack at 0.00 span, while reattachment occurred at highest angles at 0.80 span.

For each combination of nondimensional pitch rate and span location, a linear least-squares fit was applied to the instantaneous chordwise surface pressure distribution corresponding to the time when reattachment initiated. This yielded the chordwise surface pressure gradient at reattachment initiation. Results are summarized in Fig. 7 as a plot of reattachment chordwise surface pressure gradient vs nondimensional pitch rate. The surface pressure gradient at reattachment initiation became less adverse with increasing nondimensional pitch rate at all span locations. While surface pressure gradients corresponding to most conditions were adverse, those for nondimensional pitch rates 0.15 and 0.20 were predominantly favorable.

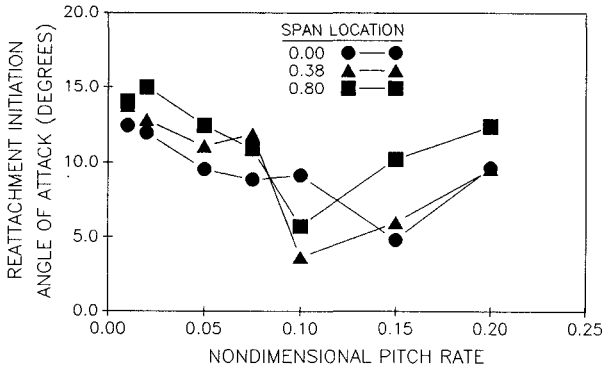

Fig. 6 Reattachment initiation angle of attack for experimental range of nondimensional pitch rate and span location.

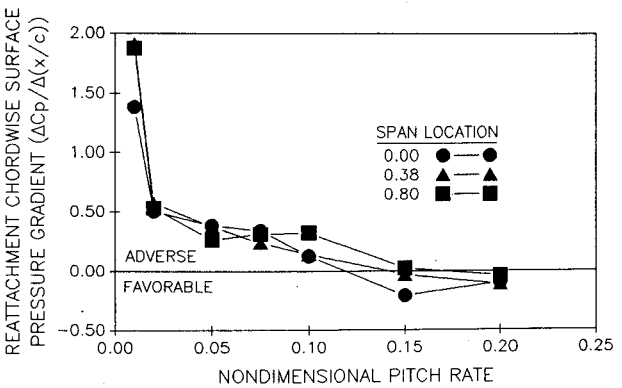

Fig. 7 Chordwise surface pressure gradient at reattachment initiation for experimental range of nondimensional pitch rate and span location.

Reattachment Progression

Linear least-squares fits were applied to reattachment progression histories like those shown in Fig. 5. This yielded a consistent determination of reattachment progression velocity, averaged over the duration of reattachment. These reattachment progression velocities are summarized in Fig. 8 as a graph of reattachment progression velocity vs nondimensional pitch rate, for three span locations. For span locations 0.38 and 0.80, maximum reattachment progression velocity occurred at nondimensional pitch rate 0.10. Lower and higher nondimensional pitch rates both resulted in lower reattachment progression velocities. For span location 0.00, at the splitter plate, highest reattachment progression velocity occurred at nondimensional pitch rate 0.05 and decreased for lower and higher nondimensional pitch rates. For the experimental range of nondimensional pitch rates, reattachment progression velocities were highest near the splitter plate and lowest near the wingtip.

Similarly, for each parameter combination, a linear least-squares fit was applied to the set of chordwise surface pressure distributions corresponding to the time interval during dynamic reattachment. This yielded the average chordwise surface pressure gradient during reattachment. These results are summarized in Fig. 9 as a plot of average chordwise surface pressure gradient vs nondimensional pitch rate. In Fig. 9, average chordwise surface pressure gradient grew less adverse with increasing nondimensional pitch rate at all span locations. For a given nondimensional pitch rate, span location 0.00 generally exhibited pressure gradients of least magnitude, while span locations farther outboard showed gradients of progressively greater magnitude. Note that all average chordwise surface pressure gradients in Fig. 9 were positive in value, signifying adverse pressure gradients.

Average reattachment progression velocities, from Fig. 8, were correlated with an average chordwise surface pressure gradient, presented in Fig. 9, for the experimental range of nondimensional pitch rate and span location. The resulting correlation is presented in Fig. 10. First-order least-squares fits were applied to the set of points corresponding to each span location. For all three span locations, adverse pressure gradients of lower magnitude (closer to zero) were associated with faster reattachment progression velocities. For any given pressure gradient, span locations nearer the splitter plate correlated with higher reattachment progression velocities. However, the slope of the first-order curve fit was steeper for span locations nearer the wingtip.

Reattachment progression velocities, from Fig. 8, were correlated with reattachment initiation angles of attack, shown in Fig. 6, for the experimental range of nondimensional pitch rate and span location. The resulting correlation is presented in Fig. 11. A second-order least-squares fit was applied to the set of points representing each span location.

For all three span locations, lower reattachment initiation angles generally resulted in higher reattachment progression velocities. However, the slopes of all three curves decrease dramatically near the upper ends. This indicates that, at low reattachment initiation angles, reattachment initiation angle exercised an attenuated influence on reattachment velocity. In addition, curve-fit slope is generally steeper for span locations nearer the splitter plate. This indicates that reattachment velocity was most sensitive to initiation angle near the splitter plate. Finally, for any given reattachment initiation angle, span locations nearer the splitter plate generally exhibited faster reattachment velocities. However, for reattachment initiation angles above 12.4 deg, the curve fits showed that reattachment progressed at highest velocity at span locations nearer the wingtip. Note that reattachment initiated above 12.4 deg only for nondimensional pitch rates 0.01 and 0.02.

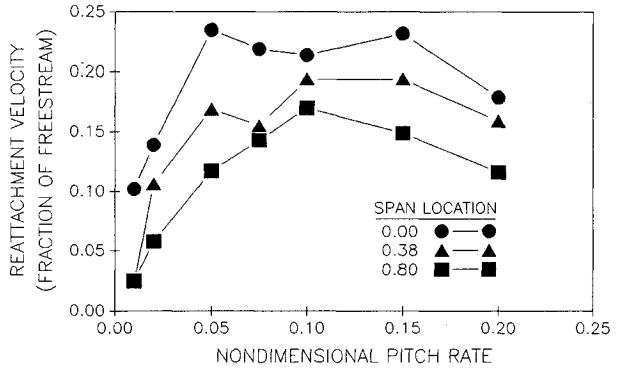

Fig. 8 Average reattachment progression velocity for experimental range of nondimensional pitch rate and span location.

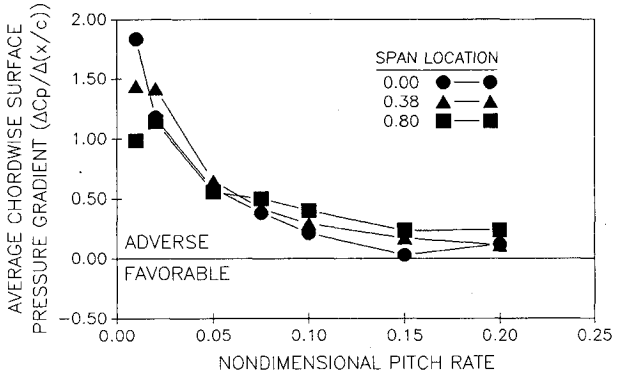

Fig. 9 Average chordwise surface pressure gradient for experimental range of nondimensional pitch rate and span location.

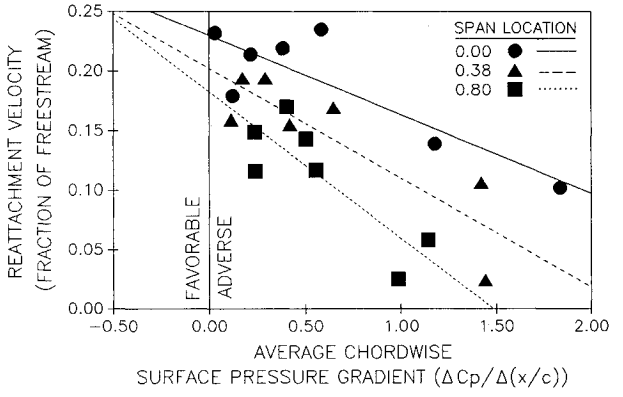

Fig. 10 Correlation of average reattachment progression velocity and average chordwise surface pressure gradient for experimental range of nondimensional pitch rate and span location.

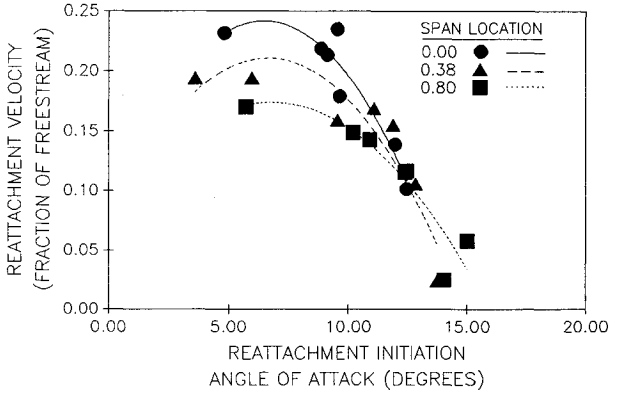

Fig. 11 Correlation of reattachment progression velocity and reattachment initiation angle of attack for experimental range of nondimensional pitch rate and span location.

Normal Force Coefficients

Figure 12 contains a representative graph of normal force coefficient vs nondimensional time for nondimensional pitch rates 0.02–0.20, at 0.375 span. Downward pitching and data acquisition both began at nondimensional time 0.0. Normal force was initially 1.37 for all nondimensional pitch rates and span locations and decreased linearly in response to downward wing pitching. Depending upon nondimensional pitch rate, linear normal force decrease underwent one of three interruption modes. For nondimensional pitch rates 0.01 (not shown) and 0.02, the linear decline ceased at some positive value of normal force, briefly rose, and finally decreased to zero normal force. For nondimensional pitch rate 0.05, normal force decreased to a slightly negative value, briefly rose to a small positive value, and soon decreased to zero. For nondimensional pitch rates 0.075–0.20, the linear decline was interrupted at negative normal force and then rose to zero.

Figure 13 is a summary plot showing the angle of attack at which linear normal force decrease was interrupted, yielding an absolute or local minimum, for the experimental range of span location and nondimensional pitch rate. Data points are absent for nondimensional pitch rates 0.01 and 0.02 at 0.80 span. At these two conditions, normal force attained no local minimum prior to reaching and stabilizing at zero. Minimum normal force angle of attack exhibited a minimum, for all span locations, at nondimensional pitch rate 0.075. Minimum normal force angles of attack were higher for both higher and lower nondimensional pitch rates. Span location 0.80 generally showed the lowest minimum normal force angle of attack over the nondimensional pitch rate range.

Figure 14 is a summary plot showing minimum normal force coefficients corresponding to the angles of attack identified in Fig. 13. As in Fig. 13, data points are absent for nondimensional pitch rates 0.01 and 0.02 at 0.80 span. Minimum normal force decreased monotonically with nondimensional pitch rate, being positive for nondimensional pitch rates 0.01 and 0.02, and negative for the remaining nondimensional pitch rates. Throughout the nondimensional pitch rate range, normal force minima were lowest at 0.00 span and decreased for 0.38 and 0.80 span.

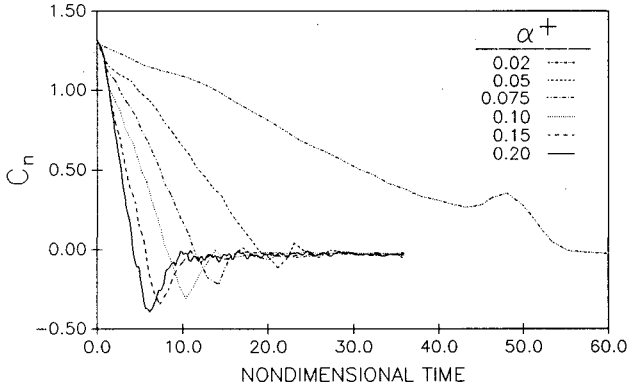

Fig. 12 Unsteady normal force coefficient histories at 0.80 span.

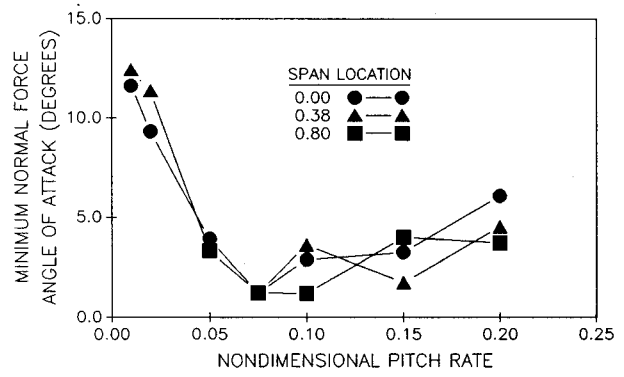

Fig. 13 Minimum normal force angle of attack for experimental range of nondimensional pitch rate and span location.

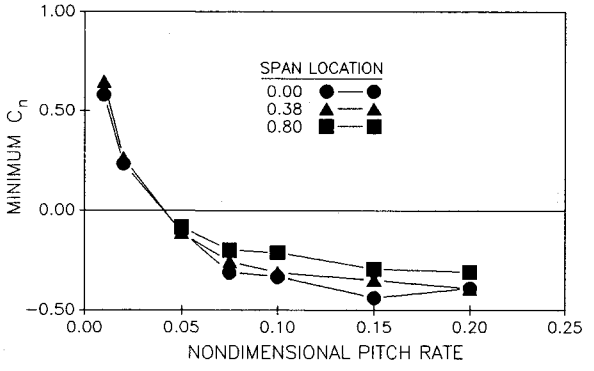

Fig. 14 Minimum normal force coefficient for experimental range of nondimensional pitch rate and span location.

Discussion

Pitching Motions

Temporal and spatial fluctuations of considerable magnitude were observed in upper surface pressure and normal force histories. In contrast, Fig. 2 showed that the rigid wing-splitter plate combination pitched at constant rate in an uninterrupted fashion. Thus, kinematic or geometric anomalies did not contribute to these prominent temporal and spatial variations.

Surface Pressure Analysis

Surface pressure data unambiguously confirmed the convective nature of dynamic reattachment on the downward pitching wing. Figure 3 showed three instantaneous upper surface pressure distributions during dynamic reattachment. In this data format, dynamic reattachment was indicated by the restoration of the chordwise surface pressure gradient that progressed towards the wing trailing edge. The same unsteady upper surface pressure data were presented as surface pressure histories in Fig. 4. As dynamic reattachment successively passed each pressure port, it appeared as a surface pressure maximum prior to pressure reduction prompted by flow reattachment. Figure 5 showed that dynamic reattachment progressed steadily aftward towards the trailing edge, beginning at 0.28 chord. As dynamic reattachment progressed aftward, it exhibited variations in instantaneous velocity during convection.

Reattachment Initiation

Figure 6 showed that initiation angle of attack varied with both nondimensional pitch rate and span location. As nondimensional pitch rate increased, reattachment initiation was delayed to progressively lower angles of attack. However, at nondimensional pitch rate 0.15, this trend reversed, with higher nondimensional pitch rates prompting reattachment initiation sooner, at higher angles of attack. Figure 7 demonstrated that the pressure gradient was predominantly favorable at these nondimensional pitch rates, and exercised a net accelerating influence on reattachment initiation.

Reattachment Progression

Reattachment progression velocity varied prominently and consistently with nondimensional pitch rate and span location, as shown in Fig. 8. For nondimensional pitch rates from 0.01 to 0.10 at span location 0.38, reattachment progression velocities showed close agreement with previous results for two-dimensional airfoils.[12,13] Correlations presented in Figs. 10 and 11 suggested physical mechanisms to account for observed trends in reattachment progression velocity.

Figure 10 demonstrated that, for all span locations, reattachment progressed faster in the presence of more attenuated

adverse chordwise pressure gradients. Span locations nearer the splitter plate exhibited higher reattachment progression velocities for a given pressure gradient. However, span locations nearer the wingtip were more responsive to changes in chordwise surface pressure gradient, as shown by the steeper curve fit slope.

Figure 11 showed that, for all span locations, reattachment progressed faster when it initiated at lower angles of attack. This observation is consistent with an empirical model constructed by Luttges and Kennedy.[17] At positive angles of attack, the region above the wing upper surface was shielded from the direct influence of the oncoming freestream. The depth of this shielded volume corresponded to the distance between the wing upper surface and a plane parallel to the freestream passing through the wing leading edge. This region grew shallower as downward pitching progressed. As this region grew shallower, reattachment structures and processes on the wing upper surface experienced increasing exposure to the freestream flow. Stronger freestream influence, in turn, drove reattachment downstream at a faster velocity.

Figure 11 also showed that, for reattachment initiation angles below 12.4 deg (corresponding to nondimensional pitch rates 0.05–0.20), reattachment velocity was higher for span locations closer to the splitter plate. In contrast, for reattachment initiation angles above 12.4 deg (corresponding to nondimensional pitch rates 0.01 and 0.02), reattachment velocity was higher for span locations nearer the wingtip. Overall, span locations nearer the splitter plate also exhibited a greater responsiveness to increments in initiation angles of attack, consistent with steeper curve fit slopes. These trends imply that three dimensionality in the reattaching flowfield amplified the freestream influence near the splitter plate.

One mechanism capable of introducing pronounced three dimensionality in unsteady flowfields is the effective angle-of-attack distribution induced by streamwise vorticity concentrated near the wingtip.[18] Figures 12 and 14 show that dynamic reattachment occurred while normal forces were positive for nondimensional pitch rates 0.01 and 0.02. This would generate downwash and attenuate wing shielding most strongly near the wingtip. This, in turn, would accelerate reattachment progression most vigorously near the wingtip, consistent with Fig. 11. In contrast, at nondimensional pitch rates 0.05–0.20, dynamic reattachment generally occurred while normal forces were negative. Upwash would result, amplifying shielding near the wingtip. This, in turn, would slow reattachment progression most near the wingtip, also consistent with Fig. 11.

Normal Force Coefficients

Figure 12 contained representative normal force histories that recorded negative normal force levels at positive angles of attack. This result is consistent with previous two-dimensional experiments where negative normal forces at positive angles of attack were attributed to temporary dominance of lower surface attached flow and effective angle-of-attack influences.[13]

Figure 13 showed that minimum normal force exhibited considerable three-dimensionality, and that minimum normal force angle of attack exhibited a trend with nondimensional pitch rate similar to that shown in Fig. 6 for reattachment initiation angle of attack. Comparison of Figs. 6 and 13 reveals that reattachment initiation preceded minimum normal force attainment, indicating that normal force continued to decline even though reattachment had begun.

Figure 14 showed a variation of minimum normal force with nondimensional pitch rate and span location. Normal force minima were higher for lower nondimensional pitch rates, where shorter delays in reattachment initiation precluded lower surface dominance of normal force. In contrast, negative normal force minima occurred at elevated nondimensional pitch rates when substantial reattachment initiation delays allowed the lower surface to dictate normal force production.

In Fig. 14, the largest difference in minimum normal force across the wingspan was 0.14 for nondimensional pitch rates 0.05–0.20. For dynamic separation, the maximum difference in stall normal force, for an identical wing-splitter plate configuration in the same nondimensional pitch rate range and span region, was approximately 1.2.[7] Thus, dynamic reattachment is significantly more two dimensional than dynamic separation.

In addition, for an identical wing-splitter plate subjected to the same nondimensional pitch rate range, normal force and surface pressure magnitudes were significantly smaller during dynamic reattachment than during dynamic separation.[4,7] Lower normal force and surface pressure magnitudes indicate that less vorticity is accumulated over the wing during dynamic reattachment than during dynamic separation.[17,19]

That dynamic reattachment is characterized by greater two dimensionality and reduced vorticity accumulations, compared to dynamic separation, is consistent with previous research by Schreck and Helin.[7] This work concluded that the mutual influence between vortices and accumulations of vorticity amplifies three dimensionality in dynamically separating flows.

Conclusions

A three-dimensional wing-splitter plate configuration was pitched downward at a constant rate from full stall at elevated angle of attack to zero angle. The resulting three-dimensional, dynamically reattaching flowfield was quantitatively characterized using unsteady surface pressures and normal force histories. Data revealed orderly alterations in reattachment initiation and progression in response to varying nondimensional pitch rate and span location. Three-dimensional normal force loading also exhibited systematic variations across the parameter range investigated. Fluid dynamic mechanisms were postulated to account for some prominent aspects of dynamic reattachment.

Dynamic reattachment initiation is strongly governed by chordwise surface pressure gradients. At elevated nondimensional pitch rate, favorable pressure gradients intervene and accelerate dynamic reattachment, prompting occurrence at higher angles of attack.

Dynamic reattachment is driven aftward on the wing principally by freestream influence, and progresses aftward at a faster rate in response to greater exposure to the freestream. Dynamic reattachment progression is impeded by adverse chordwise surface pressure gradient.

Dynamic reattachment progression varies along the wingspan. One contributor to this three dimensionality is upwash or downwash generated by streamwise vorticity near the wingtip. Differing susceptibilities to influences operating both near the wing surface and above it also point to three dimensionality in the reattaching flowfield structure.

Dynamic reattachment accumulates less total vorticity over the wing than dynamic separation. Lower total vorticity accumulation attenuates mutual interactions between concentrations of vorticity and renders dynamic reattachment more two dimensional than dynamic separation.

This experiment has provided characterization and comprehension of some aspects of three-dimensional dynamic reattachment. Further investigation of this phenomenon for more practical configurations and under conditions more representative of the full-scale flight regime are essential. This understanding, combined with existing knowledge of dynamic separation, will facilitate control and exploitation of unsteady separated flows.

Acknowledgments

The authors would like to express their appreciation to Steve Ramsey and Bobby Hatfield for their invaluable technical assistance throughout the course of this project.

References

[1]Robinson, M., Helin, H., Gilliam, F., Russell, J., and Walker, J., "Visualization of Three-Dimensional Forced Unsteady Separated Flow," AIAA Paper 86-1066, May 1986.

[2]Freymuth, P., Finaish, F., and Bank, W., "Three-Dimensional Vortex Systems of Finite Wings," *Journal of Aircraft,* Vol. 25, No. 10, 1988, pp. 971, 972.

[3]Gad-el-Hak, M., and Ho, C.-M., "Three-Dimensional Effects on a Pitching Lifting Surface," AIAA Paper 85-0041, Jan. 1985.

[4]Robinson, M., Walker, J., and Wissler, J., "Unsteady Surface Pressure Measurements on a Pitching Rectangular Wing," *Proceedings of Workshop II on Unsteady Separated Flow*, U.S. Air Force Academy, Colorado Springs, CO, 1988, pp. 225–237.

[5]Schreck, S., Addington, G., and Luttges, M., "Flow Field Structure and Development near the Root of a Straight Wing Pitching at Constant Rate," AIAA Paper 91-1793, June 1991.

[6]Lorber, P. F., "Tip Vortex, Stall Vortex, and Separation Observations on Pitching Three-Dimensional Wings," AIAA Paper 93-2972, July 1993.

[7]Schreck, S., and Helin, H., "Unsteady Vortex Dynamics and Surface Pressure Topologies on a Pitching Wing," *Journal of Aircraft*, Vol. 31, No. 4, 1994, pp. 899–907.

[8]Carr, L. W., "Progress in Analysis and Prediction of Dynamic Stall," *Journal of Aircraft*, Vol. 25, No. 1, 1988, pp. 6–17.

[9]Schreck, S., Faller, W., and Luttges, M., "Neural Network Prediction of Three-Dimensional Unsteady Separated Flow Fields," *Journal of Aircraft*, Vol. 32, No. 1, 1995, pp. 178–185.

[10]Faller, W., Schreck, S., and Luttges, M., "Real-Time Prediction and Control of Three-Dimensional Unsteady Separated Flow Fields Using Neural Networks," AIAA Paper 94-0532, Jan. 1994.

[11]Faller, W., Schreck, S., and Luttges, W., "Real-Time Prediction of Three-Dimensional Dynamic Reattachment Using Neural Networks," AIAA Paper 94-2337, June 1994.

[12]Niven, A., Galbraith, R., and Herring, D., "Analysis of Reattachment During Ramp Down Tests," *Vertica,* Vol. 13, No. 2, 1989, pp. 187–196.

[13]Niven, A., and Galbraith, R., "Experiments on the Establishment of Fully Attached Aerofoil Flow from the Fully Stalled Condition During Ramp Down Motions," 17th ICAS Conf., International Council of the Aeronautical Sciences Paper 90-3.4.3, Stockholm, Sweden, Sept., 1990.

[14]Ahmed, S., and Chandrasekhara, M., "Reattachment Studies of an Oscillating Airfoil Dynamic Stall Flow Field," AIAA Paper 91-3225, Sept. 1991.

[15]Freymuth, P., "Physical Vortex Visualization as a Reference for Computer Simulation," *Vortex Methods and Vortex Motion*, Society for Industrial and Applied Mathematics, Philadelphia, PA, 1991, p. 87.

[16]Ericsson, L. E., "Pitch-Down Dynamic Stall Characteristics," AIAA Paper 94-0535, Jan. 1994.

[17]Luttges, M., and Kennedy, D., "Initiation and Use of Three-Dimensional Unsteady Separated Flows," *Proceedings of Workshop II on Unsteady Separated Flow*, U.S. Air Force Academy, Colorado Springs, CO, 1988, pp. 211–222.

[18]Burkhalter, J., "Downwash Measurements on a Pitching Canard-Wing Configuration," *Journal of Aircraft,* Vol. 30, No. 6, 1993, pp. 1005–1008.

[19]Panaras, A., "Numerical Modeling of the Vortex/Airfoil Interaction," *AIAA Journal*, Vol. 25, No. 1, 1987, pp. 5–11.